EEG source imaging by supervised learning

Reynaud Sarah
IMT Atlantique
LaTIM U1101 INSERM
Brest, France
sarah.reynaud@imt-atlantique.fr

Merlini Adrien
IMT Atlantique
Lab-STICC UMR CNRS 6285
Brest, France
adrien.merlini@imt-atlantique.fr

Ben Salem Douraied
CHU, UBO
LaTIM U1101 INSERM
Brest, France
douraied.bensalem@chu-brest.fr

Rousseau François
IMT Atlantique
LaTIM U1101 INSERM
Brest, France
francois.rousseau@imt-atlantique.fr

***Abstract*—Estimating the electrophysiological activity at the origin of electroencephalography (EEG) measurements is an ill-posed inverse problem. Several methods solve this problem by imposing different priors on the solution. Machine learning could allow to learn the inverse function directly from the data and thus make the choice of one of the multiple solutions of the inverse problem more reliable. This work is based on simulations of electrophysiologic data containing single or multiple extended sources, using the SEREEGA simulation toolbox [1]. These data are used to train a one-dimensional convolutional network (1D-CNN) and to compare the results of this learning approach to those obtained by a recurrent long short term memory (LSTM) network from the literature, and by minimum norm energy [2] (MNE) and standardized low resolution brain electromagnetic tomography [3] (sLORETA) methods. These results on simulated data are encouraging about the potential contribution of learning-based methods to the problem of spatio-temporal EEG source imaging. Additional work still needs to be done in order to also evaluate the ability of the network to generalize to real data.**

***Index Terms*—EEG, deep learning, neuroimaging, inverse problem**

I. Introduction

Electroencephalography (EEG) provides a non-invasive, millisecond time-resolved measurement of potentials generated by electrical activity in the brain using electrodes placed on the scalp. The forward model in EEG links a known brain activity, modeled by a current distribution, and EEG measurements via the *leadfield* matrix. EEG source imaging (ESI) is the estimation of the current distribution from the EEG data. It is an ill-posed inverse problem. To solve it, a prior on the activity to be estimated must be added. The choice of a prior on the source to estimate influences the final solution, may be subject to many questions and is challenging. Some type of brain activity models, such as those with extended or multiple sources, remain challenging for ESI. In this context, machine learning approaches, in particular the use of neural networks, could allow the learning of the inverse function from realistic data.

The research that led to these results was funded by the Labex CominLabs within the CYCLE project and the ANR (AI4CHILD ANR-19-CHIA-0015-01)

Some of the earliest works using machine learning for ESI focused on estimating the position of a few equivalent dipoles from one or multiple time samples of the EEG signal, using multilayer perceptrons (MLP) [4] or recurrent networks Long Short Term Memory (LSTM) [5]. Another family of approaches consists in estimating the amplitude of equivalent current dipoles (ECD) placed on vertices of the brain mesh. There are two main categories of methods, the first one focuses mainly on the spatial distribution of the ECD by estimating the current distribution for a single time sample: [6], [7], [8], while the second one aims at estimating the spatio-temporal distribution, i.e. reconstructing the distribution of the ECD for several consecutive time samples. In this case, the typical input of a network is a window of T time samples of EEG data. The output is the corresponding window of source activity. This paper focuses on the last category of approaches: spatio-temporal EEG source imaging.

One of the important aspects in designing a deep learning algorithm is how to best represent the EEG data in order to extract spatial and temporal information. By considering the EEG data as a multivariate time series, a bidirectional LSTM network can be used to estimate the activity of spatially extended sources [9]. An auto-encoder using convolutions sequentially on the different dimensions has also been proposed, as well as a network based on a spatial module (ResNet) and a temporal module (LSTM) to extract spatio-temporal information from data [10].

In this work, we investigate the use of neural networks for ESI, compared with state-of-the-art variational methods. Quantitative evaluation relying on simulated realistic data using SEREEGA [1] is performed on two different neural network architectures: an LSTM network adapted from Hecker *et al.* [9] and a one dimensional convolutional neural network. These two networks are compared to variational methods MNE and sLORETA.

The paper is structured as follows: the simulation of electrophysiological data is presented in Section II-A. The inverse problem solving methods, learning and non-learning based, are described Section II-B and II-C respectively. Section II-D

gives details about the evaluation metrics used to compare the performance of the different methods, in Section III.

II. Methods

A. Data simulation

Since direct measurement of electrophysiological brain activity is an invasive process, there is generally no ground truth data for brain activity at the source level corresponding to EEG recordings. To train neural networks in a supervised manner to solve the inverse problem, but also to evaluate the results of different ESI methods, ground truth data are needed.

The activity measured by EEG on the scalp corresponds to the activity of groups of synchronously active neurons, which can be modeled by an equivalent current dipole [11]. The relationship between the activity of each equivalent dipole, or source, at a given position in the brain and values of potential on the scalp is represented by the *leadfield* matrix according to the forward model $\tilde{\mathbf{M}} = \mathbf{GD}$, where $\tilde{\mathbf{M}} \in \mathbb{R}^{N_e \times T}$ is the distribution of noiseless potentials at N_e given positions (electrodes) on the scalp, for T time points, $\mathbf{D} \in \mathbb{R}^{N_s \times T}$ is the source distribution and $\mathbf{G} \in \mathbb{R}^{N_e \times N_s}$ is the *leadfield* matrix. The *leadfield* matrix is built out of anatomical and biophysical information about the brain and is computed by solving the forward problem, i.e. by solving Poisson's equation on the head domain. Thus, to generate synthetic pairs of EEG and brain activity data, a source distribution is generated and then projected onto the electrodes using the forward model. The simulation of a source distribution can be divided into three parts: the definition of the head model, which is based on geometrical and biophysical information about the brain, the definition of the spatial and the temporal pattern of the source activity. In this work we used mne-python [12] to create the head model and SEREEGA [1] to simulate the sources and the resulting EEG activities.

Two datasets were created: a dataset containing data for which a single extended source is active and a dataset containing data for which multiple extended sources are active. The same head model is used for both datasets.

1) Head model: The head model that was used is defined from the MRI template fsaverage (mne-python, FreeSurfer). The *leadfield* matrix is computed using a boundary element method (BEM) with three layers: brain (cortex), skull, and skin with respective conductivity values of $0.3\,\mathrm{S/m^2}$, $0.006\,\mathrm{S/m^2}$ and $0.3\,\mathrm{S/m^2}$. The cortical mesh is subsampled to create a source space with $N_s = 1284$ cortical dipole sources with an orientation fixed normal to the surface. The electrode array has $N_e = 90$ electrodes.

2) Single extended source: An extended source consists of a region of neighboring dipoles that are similarly active. In this situation, one of the challenges of ESI is to estimate not only the center of the source, but also its correct extension.

a) Spatial pattern: The spatial pattern refers to the set of active sources. An extended source is created by selecting a seed source and an extension order, and recursively adding the neighbors of the seed source to the region, as explained in [13]. Neighboring sources are sources that share a common edge in the brain mesh. We select the extension order in the range $[\![1; 5]\!]$.

TABLE I: Simulation parameters and intervals for the multi-source dataset, variability between different examples in the dataset and between different regions within an example. Parameters are sampled uniformly in the given ranges.

Parameter	Range between examples	Range between regions
Number of regions	[1;5]	$\emptyset$
Extension order	[1;5]	$\emptyset$
Amplitude [nAm]	[0.5;1.5]	[0.15;1.7]
Center [ms]	[125;375]	[87; 487]
Width [ms]	[48;51]	[43;56]

b) Temporal pattern: The temporal pattern is the temporal shape of the signal associated to each of the active sources. For the extended single source dataset, the temporal pattern is similar to that of an event related potential (ERP). It is generated using the function from the SEREEGA toolbox which corresponds to the ERP simulation. The signal is a Gaussian function in time of the form

$$f(t) = ae^{-\frac{1}{2}\left(\frac{6(t-c)}{w}\right)^2}, \tag{1}$$

defined by its amplitude a, its center c and its width $w = 6\sigma$. These parameters are randomly chosen in given ranges for each example in the dataset. All sources in a region are assigned the same temporal signal with an amplitude decreasing as a Gaussian function of the distance between the considered source and the seed source of the region.

For this simulation the amplitude is selected in the range 0.5–$1.5\,\mathrm{nAm}$, center and width are selected in ranges 0.5–$1.5\,\mathrm{ms}$ and 48–$51\,\mathrm{ms}$ respectively. Each example has a $500\,\mathrm{ms}$ duration with a sampling frequency of $512\,\mathrm{Hz}$, i.e 256 temporal samples: $\mathbf{D} \in \mathbb{R}^{N_s \times 256}$.

A noiseless EEG signal $\tilde{\mathbf{M}}$ is then generated by projecting a source distribution $\mathbf{D}$ onto the electrode space using the forward model.

3) Multiple extended sources: Another challenge of ESI is to estimate the activity of multiple (extended) sources in the brain. We therefore considered this case by simulating a dataset with one or more active extended sources.

a) Spatial pattern: The same principle as explained for the single source dataset is used to select the sources that form an active region. In this dataset, multiple seeds and extension orders are randomly selected in given ranges, to create a source distribution composed of multiple non-overlapping regions.

b) Temporal pattern: The same ERP-like Gaussian signal as for the single extended source dataset is assigned to the active sources, with the same principle of amplitude decay within a region. Variability between regions of the same source distribution is added, so that different regions of the same source distribution sample have different waveforms. Each sample has a $500\,\mathrm{ms}$ duration and a sampling rate of $512\,\mathrm{Hz}$. The parameters and intervals used for this simulation are given Table I.

4) Noise: White Gaussian noise is added to the EEG data at a given signal to noise ratio (SNR). If we write $\tilde{\mathbf{M}} \in \mathbb{R}^{N_e \times T}$ the matrix of noiseless EEG data, and $\epsilon \in \mathbb{R}^{\mathbb{N} \times \mathbb{T}}$, $\epsilon \sim \mathcal{N}(0, \mathbf{I})$ a white Gaussian noise, the SNR can be adjusted by computing

$$\mathbf{M} = \tilde{\mathbf{M}} + \frac{\epsilon}{\|\epsilon\|_F} \frac{\|\tilde{\mathbf{M}}\|_F}{\sqrt{SNR}}. \tag{2}$$

where $||.||_F$ is the Frobenius norm.

EEG data with SNRs of $30\,\mathrm{dB}$, $20\,\mathrm{dB}$ and $10\,\mathrm{dB}$ are generated as different datasets to evaluate the noise robustness of a method.

B. Supervised learning based methods to solve the inverse problem

In this work, two methods are used to study the contribution of machine learning to ESI: a bidirectional long short term memory network with $513\,400$ parameters, adapted as closely as possible from the one proposed by Hecker *et al.* [9], and a one-dimensional convolutional neural network (1D-CNN) with $7\,102\,464$ parameters. The LSTM network is composed of two bidirectional LSTM layers and a dense layer, which allows to obtain an output with the number of sources of the considered source space, from the characteristics extracted in the recurrent layers. The 1D-CNN consists of a one-dimensional convolutional layer and a dense layer. The dimension of the convolution kernels is $N_e \times 5$ to account for all EEG channels and a temporal neighborhood. The output dimension of the convolution layer is set to 4096 and the output of the dense layer is 1284 (number of sources to estimate). The two networks are trained with a cosine similarity loss function. More precisely the loss is the opposite of the mean over time instants of the cosine similarity of the estimated source distribution vector at time t and the ground truth source distribution vector at time t.

Cosine similarity does not take into account the amplitude of the data. To compute the amplitude of the estimated sources, a normalization is performed so that the EEG signals simulated from the estimated sources have the same global power at each time as the EEG data used as input to the network (global field power (GFP) scaling, method adapted from [9]).

C. Non-learning based inverse problem solving methods

Minimum norm estimates (MNE) [2] and standardized low-resolution brain electromagnetic tomography (sLORETA) [3], two methods to solve the inverse problem in EEG based on an energy minimization prior, are used here as algorithms for comparison with machine learning methods. Both methods are implemented in the mne-python library [12] and require the computation of the noise covariance of the data. To compute this covariance matrix, points of the simulated signal that correspond to noise and not to active signal are aggregated to obtain a signal containing only noise samples.

The MNE method corresponds to the use of a L_2 norm regularization term (Tikhonov regularization), the variational formulation of the inverse problem is then of the form

$$\hat{\mathbf{d}} = \underset{\mathbf{d}}{\operatorname{argmin}} \left\{ \|\mathbf{m} - \mathbf{G}\mathbf{d}\|^2 + \lambda \|\mathbf{d}\|_2^2 \right\}, \tag{3}$$

where $\mathbf{d}$ is a vector of sources at time t, $\mathbf{m}$ the corresponding EEG vector, $\mathbf{G}$ the *leadfield* matrix and λ the regularization coefficient. Appropriate λ can be computed using methods such as L-curve. In practice a common choice is to set lambda to $1/SNR^2$, that is what is done in our experiments.

D. Evaluation metrics

The purpose of the different evaluation metrics in ESI is to evaluate the spatial and temporal aspects of the solution with respect to the ground truth. For a time t_0, the source distribution is a vector of amplitudes, and for each indexed element of the vector (each source) a corresponding position in space is known. An ideal solution would allow to perfectly estimate the amplitude vector, and thus to locate the active sources at their real position.

In the case of a distribution with a single extended source, the goal is to correctly estimate the source with maximum activity, the extension of the active region and the amplitude of the activity [14], [15]. All the metrics described bellow are computed at the time of maximum activity of the ground truth seed source, except for the peak-signal-to-noise ratio (PSNR) which is computed over the entire time series.

To evaluate the ability of a method to correctly estimate the position of active sources, **localisation error** (LE) is used. It is defined by

$$LE(\mathbf{D}_{:,t_0}, \hat{\mathbf{D}_{:,t_0}}) = \|\mathbf{r_s} - \mathbf{r_{\hat{s}}}\|_2, , \tag{4}$$

which is the Euclidean distance between the true maximum source s at position $\mathbf{r_s}$ and the estimated maximum source $\hat{s}$ at position $\mathbf{r_{\hat{s}}}$. For an ideal solution, LE = 0.

To characterize the ability of a method to properly recover the extension of an active source the **area under the ROC (receiver operating characteristic) curve** (AUC) is computed. The AUC is generally used to measure the accuracy of a classifier [16]. For the source estimation problem, the absolute value of the estimated distribution is scaled between 0 and 1 and then thresholded. In this way, we have a binary classification problem where the classes are the active and inactive sources. The AUC characterizes the ability of a method to correctly estimate the source extension and not to create outliers.

The **time error** (TE) provides information about the ability of a method to correctly estimate the source waveform. The temporal error is the absolute value of the difference between the instant of maximum activity of the ground truth and the instant of maximum activity for the estimated source (instant of maximum amplitude of the estimated core source). $TE = |t_{\max} - \hat{t}_{\max}|$.

To evaluate the quality of amplitude estimation the n**ormalized mean squared error** (nMSE) and PSNR are used. The nMSE is the mean square error (MSE) between the normalized source distributions, i.e. the source distribution divided by its maximum amplitude value. Normalizing the source distribution allows for better comparison of metric values between different methods. It takes into account the estimated global pattern more than the exact amplitude values.

Metric	Aspect of the source distribution that is evaluated
Localisation Error (LE)	Localisation
normalized MSE (nMSE)	Amplitude
AUC	Extension
Time error (TE)	Temporal
PSNR (on multiple time instants)	Amplitude

TABLE II: Aspect evaluated by the different evaluation metrics.

It is also more informative since the "amplitude" estimated by different methods does not always have the same meaning.

MSE or nMSE do not provide strong information about the location error: spurious activity will have the same effect on the MSE if it is located close to the active source region as if it is far away.

The **PSNR** is computed between the normalized signals (as for the nMSE). It is computed over the entire source distribution (several temporal samples) to give information about the overall temporal activity.

For multi-sources activities, the maximum activity time of each ground truth seed source is first estimated. Then for each pair of seed s and corresponding time of maximum activity t_0, the estimated source is identified as the source with maximum amplitude in a 7th order neighborhood of the ground truth seed, at time t_0. The metrics are computed on a seed-by-seed basis in the same way as for a single seed source. The final metric value is the average of the metrics associated to each seed. The PSNR is computed in the same way as for the single source activity.

III. Results

A. Training details

Each dataset, with single and multiple sources and for each SNR value, contains $10\,000$ examples. For each experiment, 8000 examples are used for training and 2000 for validation. The optimizer used is ADAM, with a learning rate of 0.001. For the LSTM, the batch size is 8 and gradients are clipped to 1 to match the training parameters of the original paper [9]. For the 1D CNN, the batch size is 16 and the gradients are not clipped.

B. Electrophysiological source imaging of single extended source

The results are presented in Table III and an example of visualization of the source data estimated by the different methods is presented Fig. 1a.

The results obtained with the two neural networks are comparable, and are superior to those obtained with MNE and sLORETA, for all evaluated metrics. The difference is particularly visible in localization error, for which the networks have a 2-fold lower error than sLORETA. Fig. 1a also shows the better ability of the neural networks to estimate the correct source extension, which is also expressed by the AUC. The temporal shape is globally well reconstructed by all methods, but the amplitude error is smaller for the networks. This is especially true in comparison with sLORETA which does not return an amplitude in the physical sense of the source amplitude.

C. Electrophysiological source imaging of multiple extended sources

Results for multiple extended sources are presented in Table III. In addition, an example of spatial estimation for an example containing two visible sources in the left hemisphere is shown in Fig. 1b. Here again, the two networks used perform better than the MNE and sLORETA methods. Visually the two sources are well reconstructed. The extension is estimated more accurately by the CNN-1D and LSTM than by the two energy minimization methods, which struggle to reconstruct two distinct sources.

IV. Conclusion

To solve the ill-posed inverse problem of ESI, many algorithms use a prior on the brain activity to estimate. However, the choice of a realistic prior is not straightforward and influences the obtained solution. The study of extended sources, single or multiple, is an example of brain activity that remains a challenge for many methods. Deep learning methods applied to ESI allow to learn the relationship between input EEG data and output brain activity without the external addition of a prior. In order to train a network for this task, simulated data is used. In this paper, the performance of an LSTM recurrent network and a one-dimensional convolutional network are compared to state-of-the-art MNE and sLORETA methods, based on an energy minimization prior. The results on realistic synthetic data of extended sources, single or multiple, are encouraging for the use of neural networks.

In the context of learning based approaches, the choice of the architecture is important and must be well adapted to the data: both networks have similar performances but the LSTM network of Hecker *et al* has about 15 times fewer parameters than the 1D-CNN. In order to validate the effectiveness of these methods more comprehensively, evaluations on real data must also be performed to study the ability of the networks to generalize, which is essential for their clinical use. Finally, the approach studied in this article consists in supervised learning of the inverse operator. A future research direction could be to develop a more flexible variational approach [17], in particular by learning the regularization term.

References

[1] L. R. Krol, J. Pawlitzki, F. Lotte, K. Gramann, and T. O. Zander, "Sereega: Simulating event-related eeg activity," *Journal of Neuroscience Methods*, vol. 309, pp. 13–24, 2018.

[2] M. S. Hämäläinen and R. J. Ilmoniemi, "Interpreting magnetic fields of the brain: minimum norm estimates," *Medical & Biological Engineering & Computing*, vol. 32, no. 1, pp. 35–42, Jan. 1994.

[3] R. D. Pascual-Marqui, "Standardized low-resolution brain electromagnetic tomography (sLORETA): technical details," *Methods and Findings in Experimental and Clinical Pharmacology*, vol. 24 Suppl D, pp. 5–12, 2002.

[4] G. V. Hoey, J. D. Clercq, B. Vanrumste, R. V. d. Walle, I. Lemahieu, M. D'Havé, and P. Boon, "EEG dipole source localization using artificial neural networks," *Physics in Medicine and Biology*, vol. 45, no. 4, pp. 997–1011, Apr. 2000.

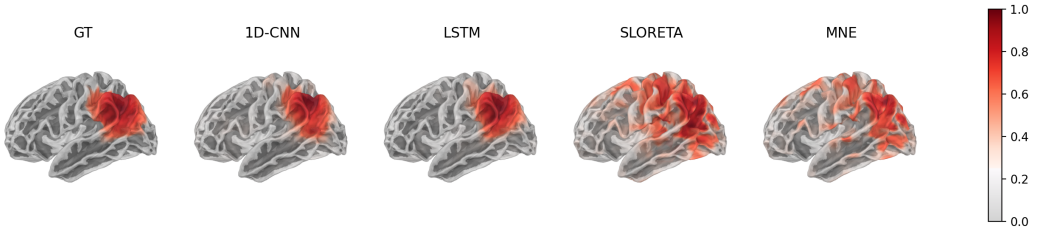

(a) Results for the case of a single extended source activity.

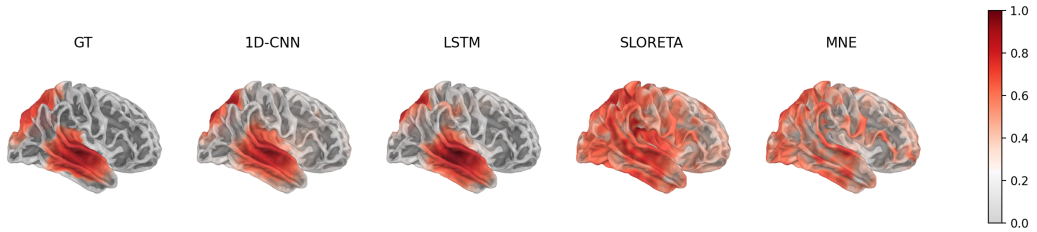

(b) Results for the case of a multiple extended source activity.

Fig. 1: Visualization of the source activity estimated by the different methods vs ground truth (GT) data. The results are thresholded so that the amplitudes lower than 25% of the maximum activity are considered inactive. For the case of multiple sources the visualized activity is the average of the activities at the maxima of each seed source.

	Methods	**Single extended source**				**Multiple extended sources**			
SNR	Metrics	1D-CNN	LSTM	MNE	sLORETA	1D-CNN	LSTM	MNE	sLORETA
30dB	AUC ↑	0.9860	**0.9878**	0.7862	0.7844	**0.7818**	0.7782	0.6600	0.6558
	LE [mm]↓	2.94	**2.45**	9.87	6.25	**4.42**	5.22	11.05	7.87
	nMSE ↓	0.0039	**0.0024**	0.0231	0.0328	0.0053	**0.0045**	0.0232	0.0375
	PSNR ↑	39.5436	**41.8593**	32.0799	29.7051	37.6688	**38.3320**	30.3987	27.6743
	time error [ms] ↓	**0.05**	0.45	1.25	1.07	**1.91**	3.23	7.42	6.61
20dB	AUC ↑	0.9859	**0.9874**	0.7847	0.7847	**0.7807**	0.7763	0.6528	0.6510
	LE [mm]↓	3.31	**2.48**	10.07	6.26	**4.76**	5.48	11.87	8.63
	nMSE ↓	0.0046	**0.0024**	0.0233	0.0354	0.0062	**0.0046**	0.0257	0.0440
	PSNR ↑	38.7850	**41.6129**	29.4784	27.5368	36.8713	**37.6045**	27.6764	25.3797
	time error [ms] ↓	**0.11**	0.46	2.62	2.00	**2.65**	5.76	15.14	10.89
10dB	AUC ↑	0.9864	**0.9892**	0.7840	0.7872	**0.7786**	0.7761	0.6459	0.6461
	LE [mm]↓	3.31	**2.52**	10.29	6.37	**5.11**	5.77	12.93	9.84
	nMSE ↓	0.0051	**0.0024**	0.0267	0.0417	0.0082	**0.0050**	0.0309	0.0550
	PSNR ↑	37.8922	**39.7914**	26.2729	24.3173	33.9728	**34.4751**	24.7509	22.3054
	time error [ms] ↓	**0.32**	0.51	5.22	3.82	**8.09**	13.45	25.86	18.28

TABLE III: Evaluation of inverse problem solving methods for both datasets.

[5] S. Cui, L. Duan, B. Gong, Y. Qiao, F. Xu, J. Chen, and C. Wang, "EEG source localization using spatio-temporal neural network," *China Communications*, vol. 16, no. 7, pp. 131–143, Jul. 2019.

[6] L. Hecker, R. Rupprecht, L. Tebartz Van Elst, and J. Kornmeier, "ConvDip: A Convolutional Neural Network for Better EEG Source Imaging," *Frontiers in Neuroscience*, vol. 15, p. 569918, Jun. 2021.

[7] C. Wei, K. Lou, Z. Wang, M. Zhao, D. Mantini, and Q. Liu, "Edge sparse basis network: A deep learning framework for eeg source localization," in *2021 International Joint Conference on Neural Networks (IJCNN)*, 2021, pp. 1–8.

[8] R. Sun, A. Sohrabpour, S. Ye, and B. He, "SIFNet: Electromagnetic Source Imaging Framework Using Deep Neural Networks," Bioengineering, preprint, May 2020.

[9] L. Hecker, R. Rupprecht, L. T. v. Elst, and J. Kornmeier, "Long-Short Term Memory Networks for Electric Source Imaging with Distributed Dipole Models," bioRxiv, Tech. Rep., Apr. 2022.

[10] R. Sun, A. Sohrabpour, G. A. Worrell, and B. He, "Deep neural networks constrained by neural mass models improve electrophysiological source imaging of spatiotemporal brain dynamics," *Proceedings of the National Academy of Sciences*, vol. 119, no. 31, p. e2201128119, Aug. 2022.

[11] B. Hanna, "Denoising, separation and localization of EEG sources in the context of epilepsy," Ph.D. dissertation, Nice Sophia Antipolis, 2014.

[12] A. Gramfort, M. Luessi, E. Larson, D. A. Engemann, D. Strohmeier, C. Brodbeck, R. Goj, M. Jas, T. Brooks, L. Parkkonen, and M. S. Hämäläinen, "MEG and EEG data analysis with MNE-Python," *Frontiers in Neuroscience*, vol. 7, no. 267, pp. 1–13, 2013.

[13] C. Grova, J. Daunizeau, J.-M. Lina, C. Bénar, H. Benali, and J. Gotman, "Evaluation of EEG localization methods using realistic simulations of interictal spikes," *NeuroImage*, vol. 29, no. 3, pp. 734–753, Feb. 2006.

[14] O. Hauk, M. Stenroos, and M. S. Treder, "Towards an objective evaluation of eeg/meg source estimation methods – the linear approach," *NeuroImage*, vol. 255, p. 119177, 2022.

[15] J. G. Samuelsson, N. Peled, F. Mamashli, J. Ahveninen, and M. S. Hämäläinen, "Spatial fidelity of MEG/EEG source estimates: A general evaluation approach," *NeuroImage*, vol. 224, p. 117430, Jan. 2021.

[16] T. Fawcett, "An introduction to ROC analysis," *Pattern Recognition Letters*, vol. 27, no. 8, pp. 861–874, Jun. 2006.

[17] R. Fablet, B. Chapron, L. Drumetz, E. Mémin, O. Pannekoucke, and F. Rousseau, "Learning Variational Data Assimilation Models and Solvers," *Journal of Advances in Modeling Earth Systems*, vol. 13, no. 10, Oct. 2021.